HHS Public Access

Author manuscript

Science. Author manuscript; available in PMC 2020 June 20.

Published in final edited form as:

Science. 2019 April 26; 364(6438): 395–399. doi:10.1126/science.aav9739.

PAC, an evolutionarily conserved membrane protein, is a proton-activated chloride channel

Junhua Yang[1,†], **Jianan Chen**[1,†], **Maria del Carmen Vitery**[1,†], **James Osei-Owusu**[1], **Jiachen Chu**[1], **Haiyang Yu**[2], **Shuying Sun**[3], **Zhaozhu Qiu**[1,4,*]

[1]Department of Physiology, Johns Hopkins University School of Medicine, Baltimore, Maryland 21205, USA.

[2]Ludwig Institute for Cancer Research, University of California at San Diego, La Jolla, CA 92093, USA.

[3]Department of Pathology, Brain Science Institute, Johns Hopkins University School of Medicine, Baltimore, Maryland 21205, USA.

[4]Solomon H. Snyder Department of Neuroscience, Johns Hopkins University School of Medicine, Baltimore, Maryland 21205, USA.

Abstract

Severe local acidosis causes tissue damage and pain, and is one of the hallmarks of many diseases including ischemia, cancer, and inflammation. However, the molecular mechanisms of the cellular response to acid are not fully understood. We performed an unbiased RNA interference screen and identified *PAC (TMEM206)* as being essential for the widely observed proton-activated Cl^- (PAC) currents ($I_{Cl,\,H}$). Overexpression of human PAC in *PAC* knockout cells generated $I_{Cl,\,H}$ with the same characteristics as the endogenous ones. Zebrafish PAC encodes a PAC channel with distinct properties. Knockout of mouse *Pac* abolished $I_{Cl,\,H}$ in neurons and attenuated brain damage after ischemic stroke. The wide expression of PAC suggests a broad role for this conserved Cl^- channel family in physiological and pathological processes associated with acidic pH.

Chloride is the most abundant free anion in animal cells and Cl^- channels have fundamental roles in physiology and disease (1). One type of Cl^- channels is activated by extracellular acidic pH. The acid- or proton-activated Cl^- (PAC) currents are present in a wide range of mammalian cells (2). Although the threshold to elicit $I_{Cl,\,H}$ is relatively low (~ pH 5.5) at room temperature (RT), the channels become activated under less acidic conditions (~ pH 6.0) at 37°C (3, 4). Tissue pH can fall below 6.0 under many pathological conditions (5–7), such as ischemic stroke, in which acidosis is thought to be an important mechanism

†Corresponding author. zhaozhu@jhmi.edu.
*These authors contributed equally to this work.

Author contributions: Z.Q. conceived the study, performed the RNAi screen, generated *PAC* KO cells, and wrote the paper with J.Y. J.Y. performed electrophysiological recordings. J.Chen implemented the stroke model. M.C.V. generated Pac KO mice and conducted the neuronal cell death assay. J.O.-O. and S.S. carried out molecular cloning. J.O.-O. performed immunostaining and the HEK cell death assay. J. Chu performed neuronal recording. H.Y. performed ES cell electroporation.

Competing interests: None declared.

Data and materials availability: All data are available in the main text or the supplementary materials.

promoting neuronal death and brain injury (8, 9). By mediating Cl^- influx and subsequent cell swelling, the non-inactivating $I_{Cl,\,H}$ have been implicated in acidosis-induced cell death (4, 10). The proton-activated Cl^- channel displays characteristic biophysical properties (2), including a strong outwardly rectifying current-voltage (*I-V*) relationship (hence the channel is also referred to as ASOR for acid-sensitive outwardly rectifying anion channel) (10), time-dependent activation at positive membrane potentials, and an anion permeability sequence of $I^- > Br^- > Cl^-$. Previous candidate gene approaches focusing on known Cl^- channel families have failed to identify the protein underlying $I_{Cl,\,H}$ (2, 3, 11), so its molecular identity has remained elusive.

To search for genes encoding the proton-activated Cl^- channel, we established a high-throughput cell-based fluorescence assay for $I_{Cl,\,H}$ activity (12). Human embryonic kidney 293 (HEK293) cells stably expressing the iodide-sensitive yellow fluorescent protein (YFP) were stimulated with acidic pH solutions to elicit the endogenous $I_{Cl,\,H}$ (13). I^- influx through the proton-activated Cl^- channel triggered a rapid fluorescence decrease (Fig. 1A). The degree of fluorescence quenching correlated with the strength of the acidic stimuli (Fig. 1B). We selected pH 5.0 for the acid-induced YFP quenching assay and performed an unbiased RNAi screen with an arrayed siRNA library (4 siRNAs per gene, 1 siRNA per well) targeting 2725 human proteins predicted to have at least two transmembrane (TM) domains (a characteristic shared by all known ion channels). Although most candidate genes had only one effective siRNA, a single previously uncharacterized gene *TMEM206* (transmembrane protein 206, or C1orf75), we now call *PAC* (proton-activated Cl^- channel), stood out with 3 out of 4 siRNAs causing a decreased quenching response (> 4 standard deviations above the mean) (Fig. 1C). We confirmed the attenuation of the quenching response and reduction of mRNA level by *PAC* siRNA transfection (Fig. 1, D to F).

We used CRISPR/Cas9 technology to inactivate the *PAC* gene in HEK293 cells (fig. S1) and performed whole-cell patch clamp recording to assay $I_{Cl,\,H}$. Perfusion of acidic solutions elicited large and stable conductances in wildtype (WT) HEK293 cells (Fig. 1G). The rapid activation and inactivation upon perfusion of different pH solutions indicate direct proton binding as the likely channel gating mechanism (Fig. 1G). The currents exhibited time-dependent facilitation at positive membrane potentials and their *I-V* relationships showed a steep outward rectification (Fig. 1H). The normalized current-to-pH relationship was fitted with a Hill equation yielding a pH_{50} of 5.0 and a Hill coefficient of 4 (fig. S2A), indicating current activation by cooperative binding of protons. Furthermore, the currents were inhibited by 4,4'-diisothiocyano-2,2'-stilbenedisulfonic acid (DIDS), a known blocker of $I_{Cl,\,H}$ (fig. S2B). These features are characteristic of the widely described proton-activated Cl^- channel. $I_{Cl,\,H}$ were abolished in two independent *PAC* knockout (KO) HEK293 cell lines (Fig. 1, I to K). This effect appeared to be specific to the proton-activated Cl^- channel because the transient inward currents at −100 mV mediated by the amiloride-sensitive acid-sensing ion channel (ASIC) were unaffected (Fig. 1I). HeLa cells also expressed a typical proton-activated Cl^- channel, and deletion of *PAC* eliminated their $I_{Cl,\,H}$ (fig. S1 and S3). We conclude that PAC is an indispensable component of the proton-activated Cl^- channel or is necessary for its activation in human cells.

On the basis of hydrophobicity analysis, human PAC protein (hPAC) is predicted to have two TM domains (Fig. 2A). Its plasma membrane localization was detected by immunostaining in nonpermeabilized cells expressing hPAC tagged with FLAG in the putative TM1-TM2 loop (Fig. 2B). In contrast, C-terminal FLAG was detected only upon cell permeabilization, consistent with a topology of N and C termini of PAC both facing the cytosolic side (Fig. 2, A and B). To test whether hPAC overexpression would rescue and enhance $I_{Cl,\,H}$, we transiently transfected hPAC cDNA in *PAC* KO HEK293 cells. Perfusion of acidic bath solutions evoked robust whole-cell currents several times larger than the endogenous $I_{Cl,\,H}$ with the same properties: time-dependent facilitation, and strong outward rectification (Fig. 2, C and D). The normalized current-to-pH relationship yields a pH_{50} of 5.0 and a Hill coefficient of 4, which were identical to those of the native currents recorded at RT (Fig. 2E and fig. S2A). Like the endogenous $I_{Cl,\,H}$ (3, 4), the pH sensitivity of hPAC was also temperature-sensitive with a shift of pH_{50} (5.5) and activation threshold (~pH 6.0) to less acidic pH at 37°C (Fig. 2, E and F). Furthermore, hPAC was blocked by several $I_{Cl,\,H}$ inhibitors, including DIDS, niflumic acid (NFA) and (5-nitro-2-(3-phenylpropylamino)benzoic acid (NPPB) (fig. S4). Substitution of extracellular Na^+ with impermeable N-methyl-D-glucamine ($NMDG^+$) did not alter $I_{Cl,\,H}$, but replacing extracellular Cl^- with the impermeable anion gluconate abolished the currents (fig. S5), indicating hPAC confers an anion channel conductance. We estimated the permeability ratios from the shift in reversal potentials observed when equimolar amounts of I^-, Br^- or Cl^- were the only permeable extracellular anion (Fig. 2G). The relative permeability ($I^- > Br^- > Cl^-$) of hPAC was essentially the same as that of native $I_{Cl,\,H}$ (Fig. 2H). Therefore, the biophysical properties and pharmacological profile of hPAC fully match with those of the endogenous proton-activated Cl^- channel in human cells.

PAC might directly assemble into a channel; however it's also possible that PAC might regulate $I_{Cl,\,H}$ activity indirectly, for example by regulating channel activation or expression. To differentiate these possibilities, we used the substituted-cysteine accessibility method (SCAM) to probe channel pore positions (14). Because it has a relatively low hydrophobicity (Fig. 2A), we tested whether the highly conserved TM2 of PAC might be part of the pore-lining domain. We generated cysteine substitution mutants of eight residues (302–309) in the extracellular side of TM2 and found four of them had normal current amplitudes (fig. S6, A and B). We tested the accessibility of these functional mutants by the thiol-reactive reagent 2-sulfonatoethyl methanethiosulfonate (MTSES). Currents mediated by one of the mutants (I307C) were rapidly blocked by the bulky MTSES, which were significantly reversed only upon application of the reducing agent dithiothreitol (DTT) (fig. S6, C to E). This indicates a covalent modification of I307C by MTSES. To further analyze whether I307 is located near the putative pore, we measured I^- to Cl^- permeability ratio of I307C and its alanine substitution mutant (I307A). Although I307C was normal, I307A showed a reduction of I^- permeability compared to WT hPAC (fig. S6, F and G). Thus, PAC is an integral component of the proton-activated Cl^- channel and I307 appears to be close to the ion-conducting pathway.

Highly similar homologs of PAC (TMEM206) are widespread among vertebrates (Fig. 3A), with more divergent homologs identified in the polychaete worm Capitella teleta and the sponge Amphimedon queenslandica. Zebrafish PAC (fPAC) share 54% amino acid identity

with hPAC and its overexpression in *PAC* KO HEK293 cells generated large $I_{Cl,\,H}$ (Fig. 3B). fPAC had a very similar pH_{50} (4.8) to its human counterpart (5.0), indicating pH sensitivity of PAC family proteins is conserved in vertebrates (Fig. 3C). However, the Hill coefficient of fPAC was close to 1, suggesting independent proton binding to the channel subunits instead of the highly positive cooperativity of hPAC (Fig. 3C). fPAC also exhibited altered kinetics: the time-dependent facilitation of fPAC was slower than that of hPAC (Fig. 3, D and E); its current decay after returning to the holding potential was also slower resulting in prominent tail currents (Fig. 3B). Additionally, the preference for I^- over Cl^- of fPAC was decreased (Fig. 3, F and G). Thus, fPAC generates $I_{Cl,\,H}$ in human cells with distinct channel gating and conducting properties from those of hPAC. Together with the mutagenesis analysis (fig. S6), these results provide evidence that PAC directly forms the proton-activated Cl^- channel pore.

To explore the role of PAC in acid-induced cell death, we treated HEK293 cells with acidic solutions. pH 5.0, but not pH 7.3, treatment for 2 hours caused necrotic cell death in WT cells. In contrast, *PAC* KO cells were partially protected (fig. S7A). Overexpression of hPAC in WT cells increased their susceptibility to cell death induced by acid treatment (fig. S7B). These data suggest that PAC contributes to acid-induced cell death in HEK293 cells. Consistent with the wide presence of $I_{Cl,\,H}$, human *PAC* mRNA is expressed broadly in various tissues (15), with the highest amounts detected in the brain (Fig. 4A). Indeed, acid perfusion in the presence of amiloride induced the outwardly rectifying $I_{Cl,\,H}$ in primary mouse cortical neurons (Fig. 4B). To determine whether Pac is essential for neuronal $I_{Cl,\,H}$, we generated *Pac* KO mice (fig. S8). The homozygous mutant mice were viable and appeared mostly normal, indicating that Pac is not required for animal viability. Cortical neurons isolated from *Pac* KO mice completely lacked $I_{Cl,\,H}$ (Fig. 4, B and C), suggesting that Pac is essential for neuronal proton-activated Cl^- channel activity. *Pac* KO neurons were partially, but significantly protected from delayed cell death induced by 1-hour acid treatment (pH 5.6 and pH 6.0) (Fig. 4, D and E). To test whether $I_{Cl,\,H}$ functions in acidosis-mediated neuronal toxicity in vivo, we subjected *Pac* KO mice to permanent middle cerebral artery occlusion (pMCAO), which induced severe ischemic brain injury. Compared to their WT littermates, *Pac* KO mice exhibited significantly smaller total brain infarct volume one day after pMCAO (Fig. 4, F and G). Consistently, their neurological scores were also improved (Fig. 4H). Thus, inhibition of the proton-activated Cl^- channel appears to limit the pathogenesis of ischemic brain injury.

We identified PAC, a novel membrane protein family with no sequence similarity to other ion channels, as the proton-activated Cl^- channel. Our findings provide the basis to elucidate PAC gating mechanisms by the simplest ligand, the proton, and to identify channel modulators. Like ASIC channels (16), PAC may represent a potential drug target for stroke and other acidosis-associated diseases. The threshold for PAC activation is too acidic to be found commonly in the physiological conditions except for the endocytic pathways and secretory vesicles (a luminal pH 4.5–6.5). PAC may traffic from the plasma membrane to intracellular organelles (17), and regulate their function by modulating the luminal Cl^- concentration (18, 19). Exome sequencing of Tibetan highlanders identified *PAC* (*TMEM206*) as one of the genes with highest frequency change compared to ethnic Han Chinese individuals (20). The *PAC* genomic region is also under increased natural selection

in pigs adapted to high altitude (21). Thus, PAC could have a conserved role in the adaptation to hypoxia.

Supplementary Material

Refer to Web version on PubMed Central for supplementary material.

Acknowledgements:

We thank A. Patapoutian, W.B. Guggino, and K.W. Yau for helpful discussion; A. Orth for the siRNA library; Y. Zhou for assistance with RNAi data analysis; A. Dubin and S. Murthy for advice on electrophysiology; M. Tian for help with primary neuron culture. This paper is dedicated to the memory of our dear friend and wonderful colleague, Dr. Maria del Carmen Vitery, who recently passed away.

Funding: This work was supported by NIH grants R35 GM124824 (Z.Q.) and R01 NS107347 (S.S.); AHA fellowships 19POST34410020 (J. Chen) and 18PRE34060025 (J.O.-O.); and NIH fellowships F31 NS108658 (M.C.V.) and F32 AG059358 (H.Y.).

References and Notes

1. Duran C, Thompson CH, Xiao Q, Hartzell HC, Chloride channels: often enigmatic, rarely predictable. Annu Rev Physiol 72, 95–121 (2010). [PubMed: 19827947]
2. Capurro V et al., Functional analysis of acid-activated Cl(−) channels: properties and mechanisms of regulation. Biochim Biophys Acta 1848, 105–114 (2015). [PubMed: 25306966]
3. Sato-Numata K, Numata T, Okada T, Okada Y, Acid-sensitive outwardly rectifying (ASOR) anion channels in human epithelial cells are highly sensitive to temperature and independent of ClC-3. Pflugers Arch 465, 1535–1543 (2013). [PubMed: 23708799]
4. Sato-Numata K, Numata T, Okada Y, Temperature sensitivity of acid-sensitive outwardly rectifying (ASOR) anion channels in cortical neurons is involved in hypothermic neuroprotection against acidotoxic necrosis. Channels (Austin) 8, 278–283 (2014). [PubMed: 24476793]
5. Gatenby RA, Gillies RJ, A microenvironmental model of carcinogenesis. Nat Rev Cancer 8, 56–61 (2008). [PubMed: 18059462]
6. Lardner A, The effects of extracellular pH on immune function. J Leukoc Biol 69, 522–530 (2001). [PubMed: 11310837]
7. Siesjo BK, Katsura K, Kristian T, Acidosis-related damage. Adv Neurol 71, 209–233; discussion 234–206 (1996). [PubMed: 8790801]
8. Xiong ZG et al., Neuroprotection in ischemia: blocking calcium-permeable acid-sensing ion channels. Cell 118, 687–698 (2004). [PubMed: 15369669]
9. Nedergaard M, Goldman SA, Desai S, Pulsinelli WA, Acid-induced death in neurons and glia. J Neurosci 11, 2489–2497 (1991). [PubMed: 1869926]
10. Wang HY, Shimizu T, Numata T, Okada Y, Role of acid-sensitive outwardly rectifying anion channels in acidosis-induced cell death in human epithelial cells. Pflugers Arch 454, 223–233 (2007). [PubMed: 17186306]
11. Sato-Numata K, Numata T, Inoue R, Sabirov RZ, Okada Y, Distinct contributions of LRRC8A and its paralogs to the VSOR anion channel from those of the ASOR anion channel. Channels (Austin), 1–6 (2016).
12. Qiu Z et al., SWELL1, a plasma membrane protein, is an essential component of volume-regulated anion channel. Cell 157, 447–458 (2014). [PubMed: 24725410]
13. Lambert S, Oberwinkler J, Characterization of a proton-activated, outwardly rectifying anion channel. J Physiol 567, 191–213 (2005). [PubMed: 15961423]
14. Karlin A, Akabas MH, Substituted-cysteine accessibility method. Methods Enzymol 293, 123–145 (1998). [PubMed: 9711606]
15. Uhlen M et al., Proteomics. Tissue-based map of the human proteome. Science 347, 1260419 (2015).

16. Wemmie JA, Taugher RJ, Kreple CJ, Acid-sensing ion channels in pain and disease. Nat Rev Neurosci 14, 461–471 (2013). [PubMed: 23783197]
17. Steinberg F et al., A global analysis of SNX27-retromer assembly and cargo specificity reveals a function in glucose and metal ion transport. Nat Cell Biol 15, 461–471 (2013). [PubMed: 23563491]
18. Stauber T, Jentsch TJ, Chloride in vesicular trafficking and function. Annu Rev Physiol 75, 453–477 (2013). [PubMed: 23092411]
19. Mindell JA, Lysosomal acidification mechanisms. Annu Rev Physiol 74, 69–86 (2012). [PubMed: 22335796]
20. Yi X et al., Sequencing of 50 human exomes reveals adaptation to high altitude. Science 329, 75–78 (2010). [PubMed: 20595611]
21. Dong K et al., Genomic scan reveals loci under altitude adaptation in Tibetan and Dahe pigs. PLoS One 9, e110520 (2014).

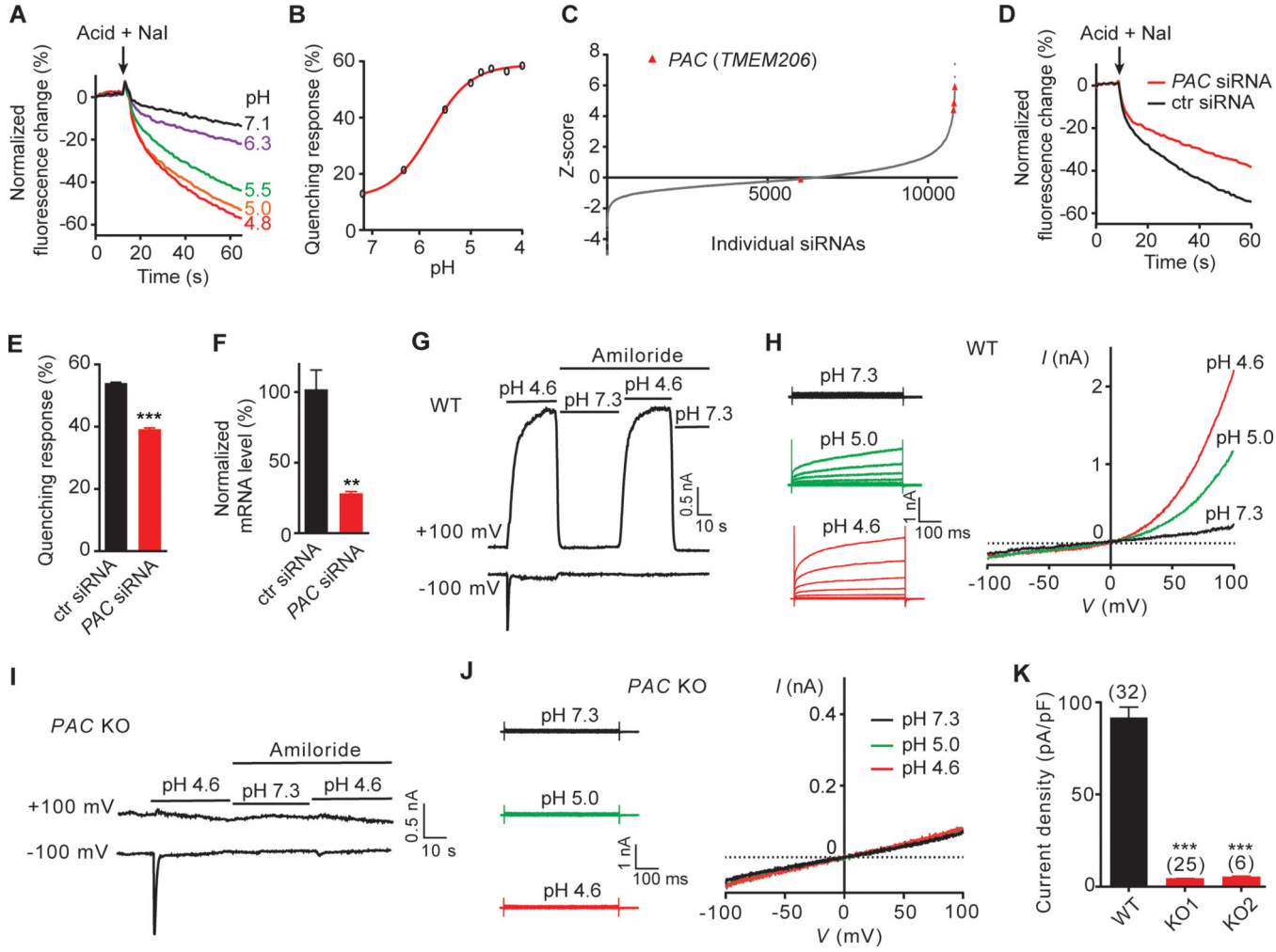

Fig. 1. RNAi screen identifies PAC as essential for the proton-activated Cl^- currents.

(A) Acid-induced and I^--dependent fluorescence change (normalized to the baseline) in HEK293-YFP cells. (**B)** Acid-induced quenching response-to-pH relationship ($n = 12$ wells). Unapparent error bars are smaller than symbols. (**C)** Z-score (the number of standard deviations from the mean) of individual siRNAs (PAC siRNAs in red) are plotted according to the rank order. See Methods for details. **(D)** Acid-induced fluorescence change, **(E)** quenching response ($n = 6$ wells), and **(F)** *PAC* mRNA knockdown ($n = 3$ wells) in HEK293-YFP cells transfected with control or *PAC* siRNA. **(G)** Whole-cell currents induced by extracellular pH 4.6 in WT HEK293 cells. The transient inward current at −100 mV is blocked by 100 μM amiloride, an ASIC channel blocker. **(H)** $I_{Cl,\,H}$ monitored by voltage step (left) and ramp (right) protocols in WT HEK293 cells. **(I)** Whole-cell currents induced by extracellular pH 4.6 in *PAC* KO HEK293 cells. Note the normal amiloride-sensitive ASIC current is apparent at −100 mV. **(J)** $I_{Cl,\,H}$ monitored by voltage step (left) and ramp (right) protocols in *PAC* KO HEK293 cells. **(K)** Current densities at +100 mV induced by extracellular pH 4.6 in WT and two *PAC* KO HEK293 cells. KO1 was used throughout the study unless stated otherwise. Data points or bars represent mean ± SEM. $^{**}P < 0.01$,

***$P < 0.001$ [Two-tailed Student's *t*-test in (E) and (F); one-way ANOVA with Bonferroni post hoc test in (K)].

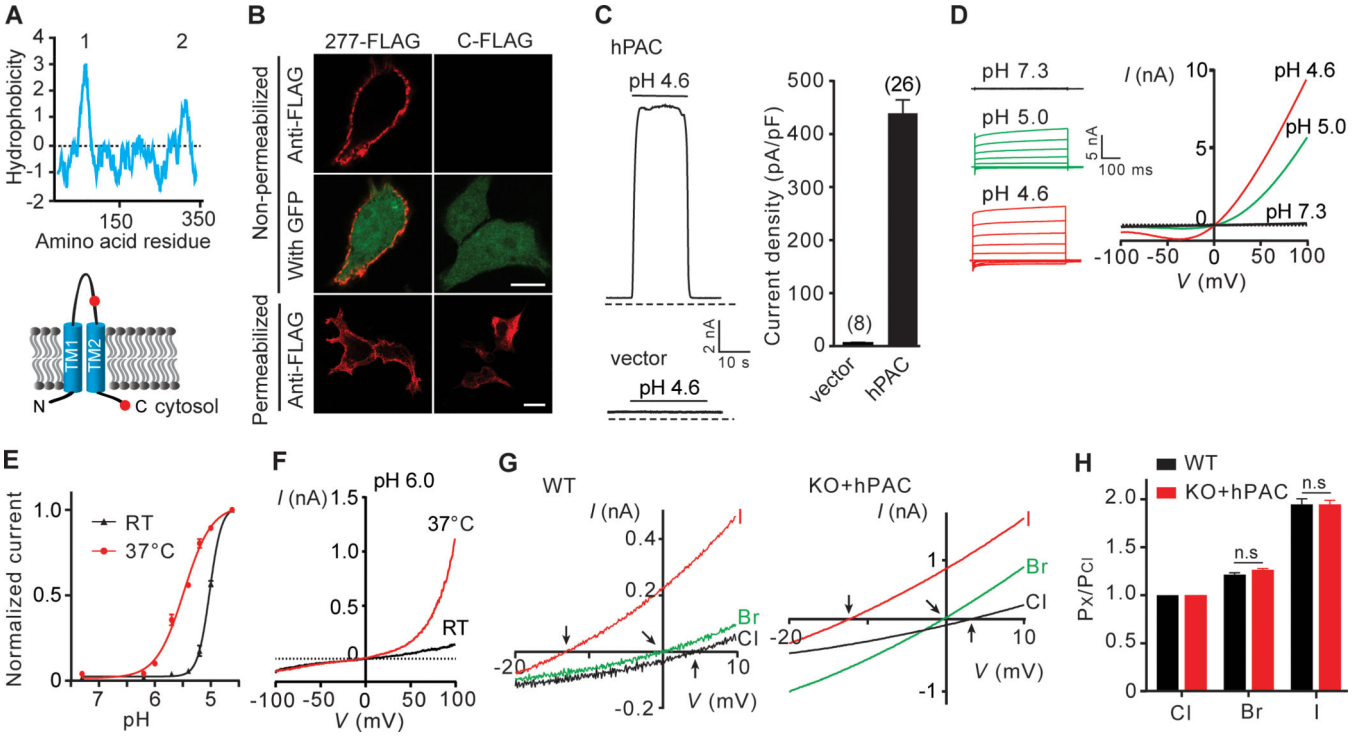

Fig. 2. Human PAC recapitulates the properties of endogenous proton-activated Cl^- channel.

(A) Hydrophobicity plot (top) and a predicted 2 TM topology (bottom) of hPAC. Red circles indicate FLAG insertion sites. **(B)** Nonpermeabilized and permeabilized HEK293 cells expressing FLAG-tagged hPAC were immunostained with anti-FLAG antibody. Scale bars: 10 μm. **(C)** Time courses (left) and current densities (right) of extracellular pH 4.6-induced whole-cell currents at +100 mV in vector or hPAC transfected *PAC* KO HEK293 cells. **(D)** hPAC-mediated currents at different pH monitored by voltage step (left) and ramp (right) protocols. **(E)** The normalized current-to-pH relationship of hPAC recorded at RT (n = 10–15 cells) or 37°C (n = 11–12 cells). Current at pH 4.6 and +100 mV is set to 1.0. **(F)** pH 6.0-induced hPAC current recorded at 37°C. **(G)** Representative I-V relationship recorded in extracellular I^-, Br^-, or Cl^- pH 4.6 solution and **(H)** anion selectivity in WT (n = 10 cells) and *PAC* KO HEK293 cells expressing hPAC (n = 14 cells). Arrows in (G) indicate the reversal potentials. Data points or bars represent mean ± SEM. n.s, not significant [two-tailed Student's t-test in (H)]

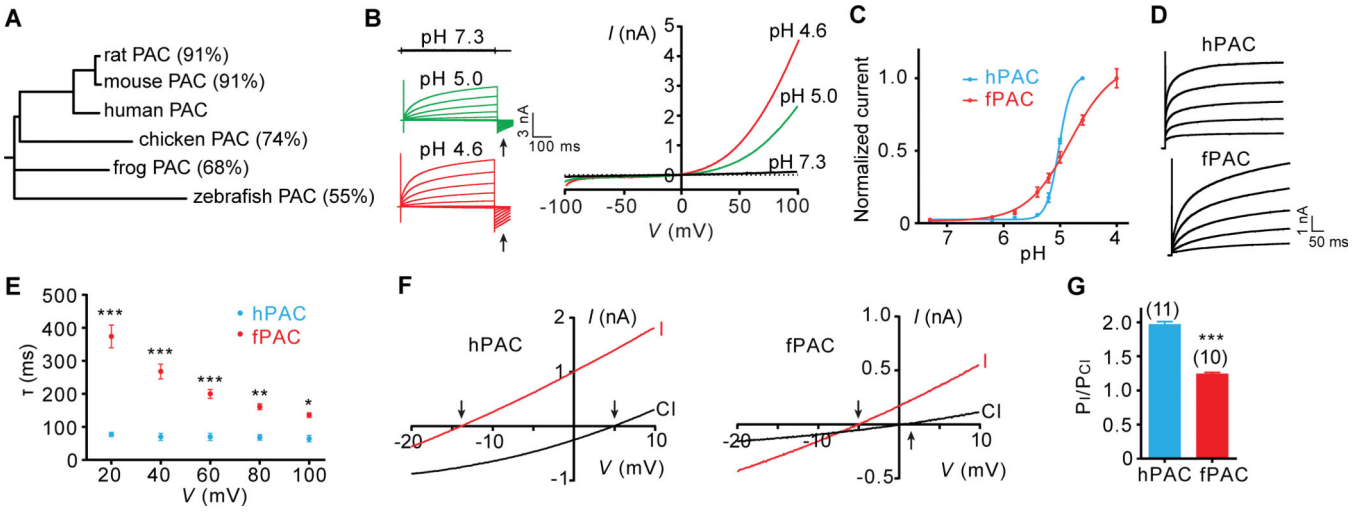

Fig. 3. Zebrafish PAC encodes a proton-activated Cl^- channel with distinct properties.

(A) Phylogenetic tree of PAC from different vertebrate animals (sequence similarity to human) generated with the ClustalW program. **(B)** fPAC-mediated currents at different pH monitored by voltage step (left) and ramp (right) protocols. Arrows point to the tail currents compared with those of hPAC (Fig. 2D). **(C)** The normalized current-to-pH relationship of hPAC (current at pH 4.6 is set to 1.0, n = 10–15 cells) and fPAC (current at pH 4.0 is set to 1.0, n = 5–12 cells) recorded at RT. **(D)** Examples and **(E)** time constant values (**τ**) of time-dependent facilitation at +20 to +100 mV voltage steps for hPAC (n = 7 cells) and fPAC (n = 11 cells). **τ** values were determined by fitting the currents with a single exponential function. **(F)** Representative *I-V* relationship recorded in extracellular pH 4.6 containing I^- or Cl^- solution and **(G)** I^- vs. Cl^- permeability for hPAC and fPAC. Arrows in (F) indicate the reversal potentials. Data points or bars represent mean ± SEM. $^*P < 0.05$, $^{**}P < 0.01$, $^{***}P < 0.001$ [two-way ANOVA with Bonferroni post hoc test in (E); two-tailed Student's *t*-test in (G)].

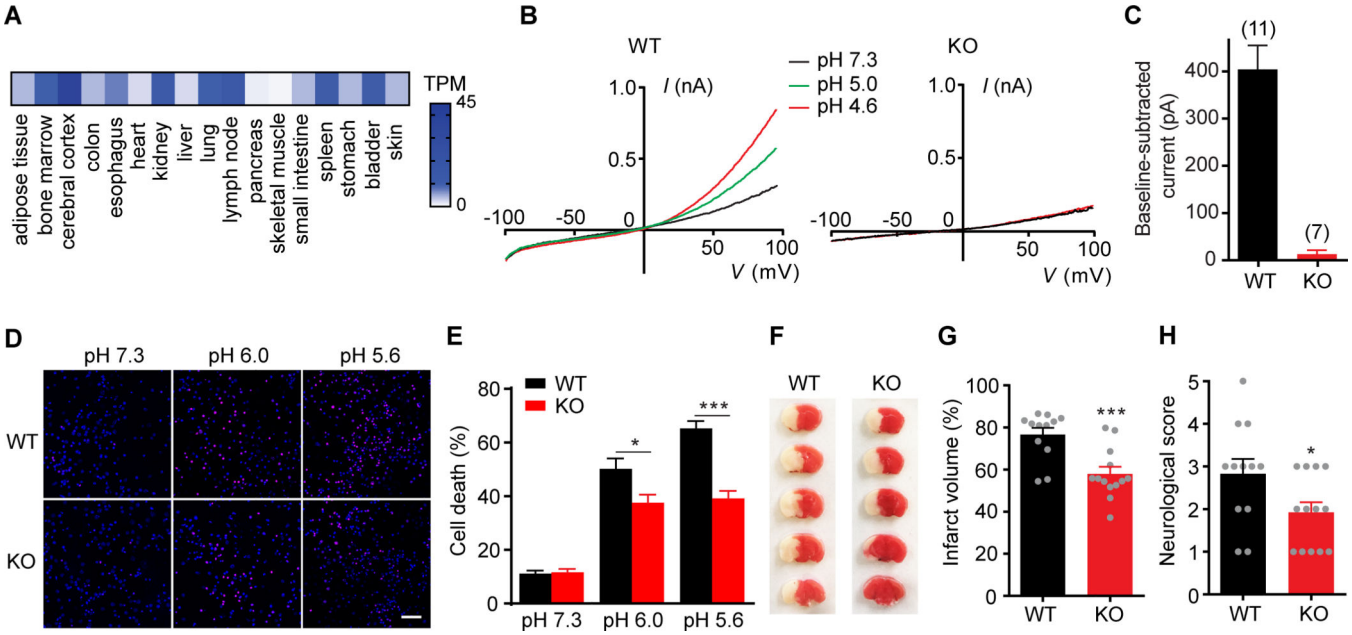

Fig. 4. PAC contributes to acid-induced cell death and ischemic brain injury

(A) TPM (transcripts per million) of *PAC* gene in selective human tissues from RNA-seq data (n = 2–7 biological replicates) (15). **(B)** $I_{Cl,\,H}$ and **(C)** baseline-subtracted pH 4.6-induced currents at +100 mV in WT or *Pac* KO primary mouse neurons. Recordings were performed in the presence of 100 μM amiloride to block ASICs. **(D)** Images of neurons stained with Hoechst 33342 (blue) for nuclei of all neurons and with propidium iodide (red) for nuclei of dead neurons. Scale bar: 50 μm. **(E)** Percent of acid-induced neuronal cell death (n = 8 wells, 1-hour acid treatment and 24-hours recovery in culture medium) (9). **(F)** Triphenyltetrazolium chloride (TTC) staining (necrotic tissue in white), **(G)** total infarct volume (normalized to total volume of the ipsilateral hemisphere as 100%), and **(H)** neurological score 1 day after permanent middle cerebral artery occlusion (pMCAO) (n = 12 and 13 for WT and *Pac* KO mice, respectively). Bars represent mean ± SEM. *$P < 0.05$, ***$P < 0.001$ [two-tailed Student's t-test in (E) and (G); Mann-Whitney U test in (H)].